ARTICLE

A 3.8-million-year-old hominin cranium from Woranso-Mille, Ethiopia

Yohannes Haile-Selassie[1,5]*, Stephanie M. Melillo[2,5]*, Antonino Vazzana[3], Stefano Benazzi[3] & Timothy M. Ryan[4]

The cranial morphology of the earliest known hominins in the genus *Australopithecus* remains unclear. The oldest species in this genus (*Australopithecus anamensis*, specimens of which have been dated to 4.2–3.9 million years ago) is known primarily from jaws and teeth, whereas younger species (dated to 3.5–2.0 million years ago) are typically represented by multiple skulls. Here we describe a nearly complete hominin cranium from Woranso-Mille (Ethiopia) that we date to 3.8 million years ago. We assign this cranium to *A. anamensis* on the basis of the taxonomically and phylogenetically informative morphology of the canine, maxilla and temporal bone. This specimen thus provides the first glimpse of the entire craniofacial morphology of the earliest known members of the genus *Australopithecus*. We further demonstrate that *A. anamensis* and *Australopithecus afarensis* differ more than previously recognized and that these two species overlapped for at least 100,000 years—contradicting the widely accepted hypothesis of anagenesis.

The absence of cranial remains of *Australopithecus* species that are older than 3.5 million years has limited our understanding of the evolutionary history of this genus. Here we describe a nearly complete hominin cranium, dated to approximately 3.8 million years (Myr) ago, that fills a crucial gap in the hominin fossil record. The specimen shows a morphology that is more primitive than that of any previously known *Australopithecus* cranium, including features that link early *Australopithecus* to the Mio-Pliocene genera *Sahelanthropus* and *Ardipithecus*. Derived features are concentrated in the face, appearing in an unexpected combination that is variably shared with *A. afarensis* and paralleling the morphology that is present in later australopiths.

Discoveries of hominin fossils in the past three decades have resulted in the naming of numerous new taxa, including the earliest species known thus far[1–11]. These discoveries have added to our understanding of human evolution by pushing the hominin fossil record into the Miocene epoch[2–4,10], and by showing possible taxonomic diversity[5,9], wider geographical distributions[1], the presence of multiple forms of bipedalism[6,12] and a major adaptive shift associated with the origin of the genus *Australopithecus*[12]. At the same time, these discoveries raise important questions related to hominin taxonomy and systematics[9,13,14]. Although most questions emanate from the fragmentary (mostly dentognathic) nature of the fossil record and small sample size, some issues relate to the absence of fossils from critical time periods and skeletal elements informative in systematics.

The Woranso-Mille study area, located in the Afar region of Ethiopia, has become one of the most important sites and has yielded hominin fossils from a poorly known period of the mid-Pliocene epoch. Since 2005, fieldwork at Woranso-Mille has been aimed at answering questions about mid-Pliocene hominin diversity and testing the hypothesized ancestor–descendant relationship of *A. anamensis* and *A. afarensis*. In this regard, Woranso-Mille hominin fossils have shown that more than one hominin species was present during the mid-Pliocene epoch (at least *A. afarensis* and an as-yet-unnamed species that is represented by the Burtele foot)[6,15]. Another species, *Australopithecus deyiremeda*, has also been named on the basis of fossils from 3.5–3.3-Myr-old deposits, even though this has been contested[13]. The 3.8–3.6-Myr-old hominin fossils—which are mostly

dentognathic—from Woranso-Mille have also corroborated the proposed ancestor–descendant relationship between *A. anamensis* (4.2–3.9 Myr ago) and *A. afarensis* (3.7–3.0 Myr ago)[16,17]. Fieldwork in 2016 resulted in the recovery of a nearly complete cranium of an early hominin (Fig. 1). This cranium (MRD-VP-1/1, hereafter MRD) was dated to 3.8 Myr ago[18] and hence comes from a critical period close to 4 Myr ago, during which the craniofacial morphology of early hominins is almost completely unknown. To our knowledge, MRD is the first specimen to shed light on the full cranial anatomy of the earliest known australopiths. Details of the discovery and preservation of the specimen are provided in Supplementary Note 1. Missing parts and minor distortions of this specimen were reconstructed digitally (Extended Data Figs. 1–5, Methods and Supplementary Notes 2–5).

Morphological descriptions

The MRD cranium has a well-developed sagittal crest and a robustly built, long and prognathic face. Its preserved right canine is among the largest known for early hominins, especially in its mesiodistal dimension. These features suggest that MRD represents a male, despite the fact that the specimen is very small in overall size. This individual had reached an advanced developmental age. The preserved postcanine teeth are heavily worn (almost to the cervico-enamel junction), except for the M[3]. Most of the sutures are obliterated on the ectocranial surface and the alveolar bone shows age-related remodelling.

The specimen is readily identifiable as a hominin by the following morphological features: the canine is reduced in size compared to non-human apes and shows a strong lingual basal tubercle; the mastoids are inflated; the nuchal plane is more horizontal than in non-human apes; and the inion, which is coincident with the opisthocranion, lies near the level of the Frankfort horizontal plane. At the same time, the small cranial capacity, highly prognathic face, extensive pneumatization and other features discussed below indicate that MRD represents a hominin that is more primitive than *A. afarensis*.

Analyses of the maxilla and dentition

The MRD canine is relatively large (compared to other hominins) and shows mesiodistal elongation. Basic dimensions align the

[1]Department of Physical Anthropology, Cleveland Museum of Natural History, Cleveland, OH, USA. [2]Department of Human Evolution, Max Planck Institute for Evolutionary Anthropology, Leipzig, Germany. [3]Department of Cultural Heritage, University of Bologna, Ravenna, Italy. [4]Department of Anthropology, Pennsylvania State University, University Park, PA, USA. [5]These authors contributed equally: Yohannes Haile-Selassie, Stephanie M. Melillo. *e-mail: yhaileselassie@cmnh.org; stephanie_melillo@eva.mpg.de
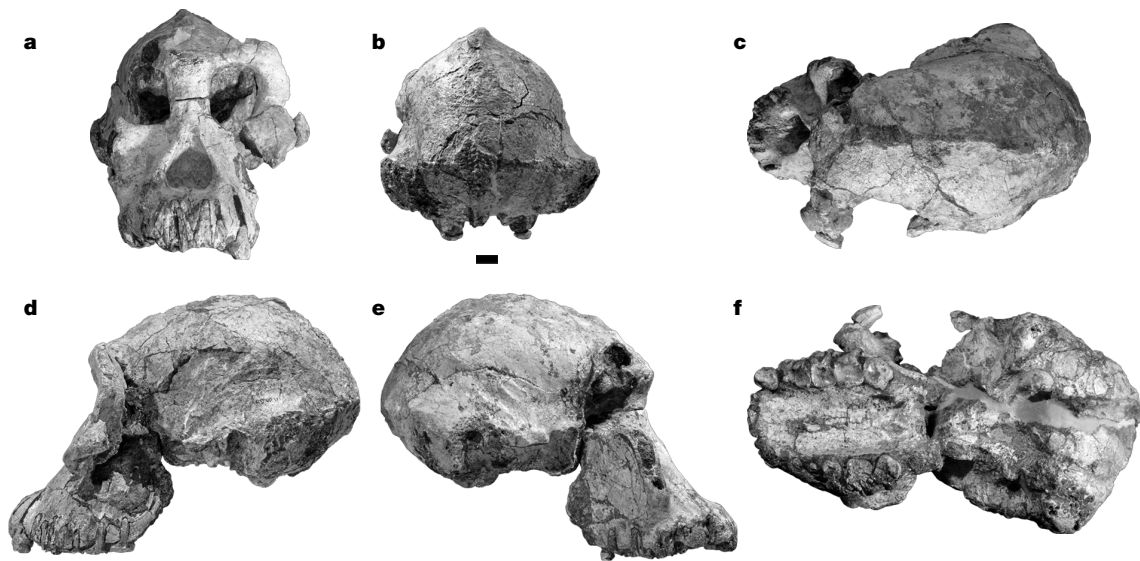
Fig. 1 | The MRD-VP-1/1 cranium. a, Anterior view. **b**, Posterior view. **c**, Superior view. **d**, Left lateral view. **e**, Right lateral view. **f**, Inferior view. The specimen is oriented in Frankfort horizontal plane. Scale bar, 1 cm.

specimen with *A. anamensis* or more-primitive hominins[19–22] (Fig. 2a, b and Supplementary Note 6). Furthermore, a number of qualitative features are shared between MRD and *A. anamensis* upper canines (Fig. 2c). The mesial and distal basal tubercles (crown 'shoulders') are short, equidistant from the cervico-enamel junction and occlusally divergent. The degree of mesiodistal elongation and short shoulders are particularly important, because they are among the few distinctive features described for *A. anamensis* that are not shared by *A. afarensis* or *Ardipithecus ramidus*[19,23]. Short mesial shoulders are, however, present in upper canines attributed to *Ardipithecus kadabba*[24] and *Orrorin tugenensis*[10]. Additional primitive features shared among the canines of MRD, *A. anamensis* and other earlier hominins are present on the lingual crown face. The lingual ridge is large, blunt and mesially offset, which relegates the mesial lingual fossa to a small slit-like structure at the mesial-most extent of the lingual face[25]. A wear facet is present on the lingual face in MRD, KNM-KP 58309 and some *A. ramidus* specimens[26]. This feature may have been produced through non-honing contact with an asymmetric and mesiobuccally bulging P_3.

Little can be said about the morphology of the other teeth, owing to damage and wear. However, even though the incisor crowns are broken off, the remaining parts of the crowns and the shape of the roots indicate that the incisors were vertically implanted. A wide (approximately 4-mm) I^2–C diastema is present in MRD. This feature is absent in the *Sahelanthropus tchadensis* cranium[3], but is variably present in *A. afarensis* and has also been documented in *A. ramidus* (for example, ARA-VP-6/500-115)[26]. The MRD canine and midface are posteriorly inclined, which is a notable difference from some of the *A. anamensis* specimens[7,19,21] (Extended Data Fig. 6 and Supplementary Note 6). The M^3 crown is sub-triangular in outline and rotated in the dental row such that the protocone–hypocone crown wall faces in the distolingual direction. The latter feature occurs commonly in *A. anamensis* specimens, but less so in *A. afarensis*.

The MRD maxillary dental arcade is relatively narrow and slightly U-shaped (Supplementary Note 6). The canine is aligned with the post-canine tooth row (Extended Data Fig. 7). The inferolateral margin of the nasal aperture in MRD is smooth and rounded owing to the confluence of a pronounced canine jugum with the nasal margin. This is also the condition that is found in *A. anamensis* specimens[19,21,25]. Most *A. afarensis* maxillae have thin lateral margins and sharp infero-lateral corners[27]. The MRD palate is very deep, a morphology that is conventionally considered to be derived. The depth at the M^1/M^2 level (17.4 mm) exceeds all known *A. anamensis* and *A. afarensis* specimens
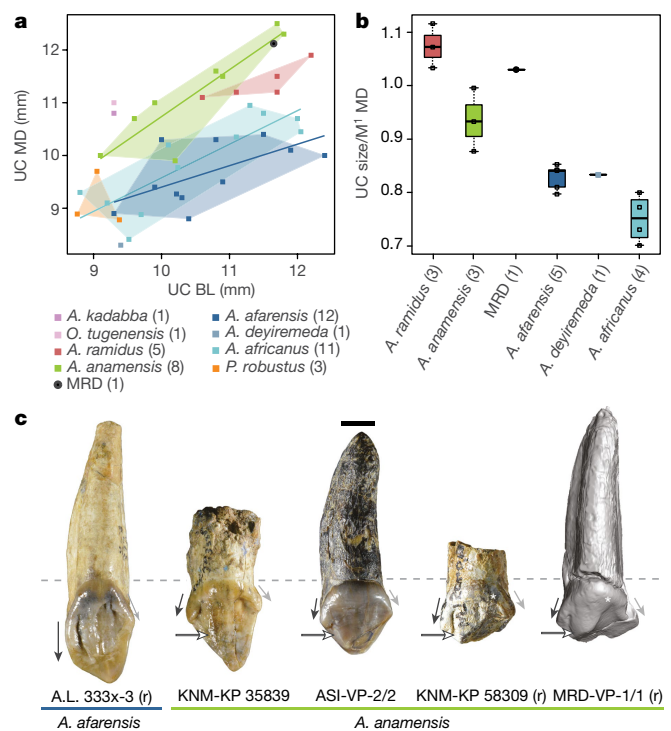

Fig. 2 | Comparisons of upper canine morphology. a, Upper canine basal dimensions. Least-squares regression lines are shown for *A. anamensis*, *A. afarensis* and *A. africanus*. BL, buccolingual; MD, mesiodistal; UC, upper canine. **b**, Relative canine size ($\sqrt{(MD \times BL)}/M^1$ MD). Box plots or individual observations are shown. The box plots show the centre line (median), box limits (upper and lower quartiles), whiskers (range) and individual values (squares). Taxa are arranged chronologically, showing the temporal trend of decreasing relative canine size. Sample sizes (*n*) are reported in parentheses after the species names. **c**, Lingual face of the canine crown in *A. afarensis* and *A. anamensis* at sequential wear stages. The length and orientation of the mesial and distal basal tubercles are illustrated by black and grey arrows, respectively. White arrows indicate a slit-like mesial lingual fossa and white asterisks mark the extension of a wear facet onto the lingual crown face. Canines are aligned at the cervical enamel line (dashed grey line). All specimens are shown as right teeth and (r) indicates images that have been reversed.
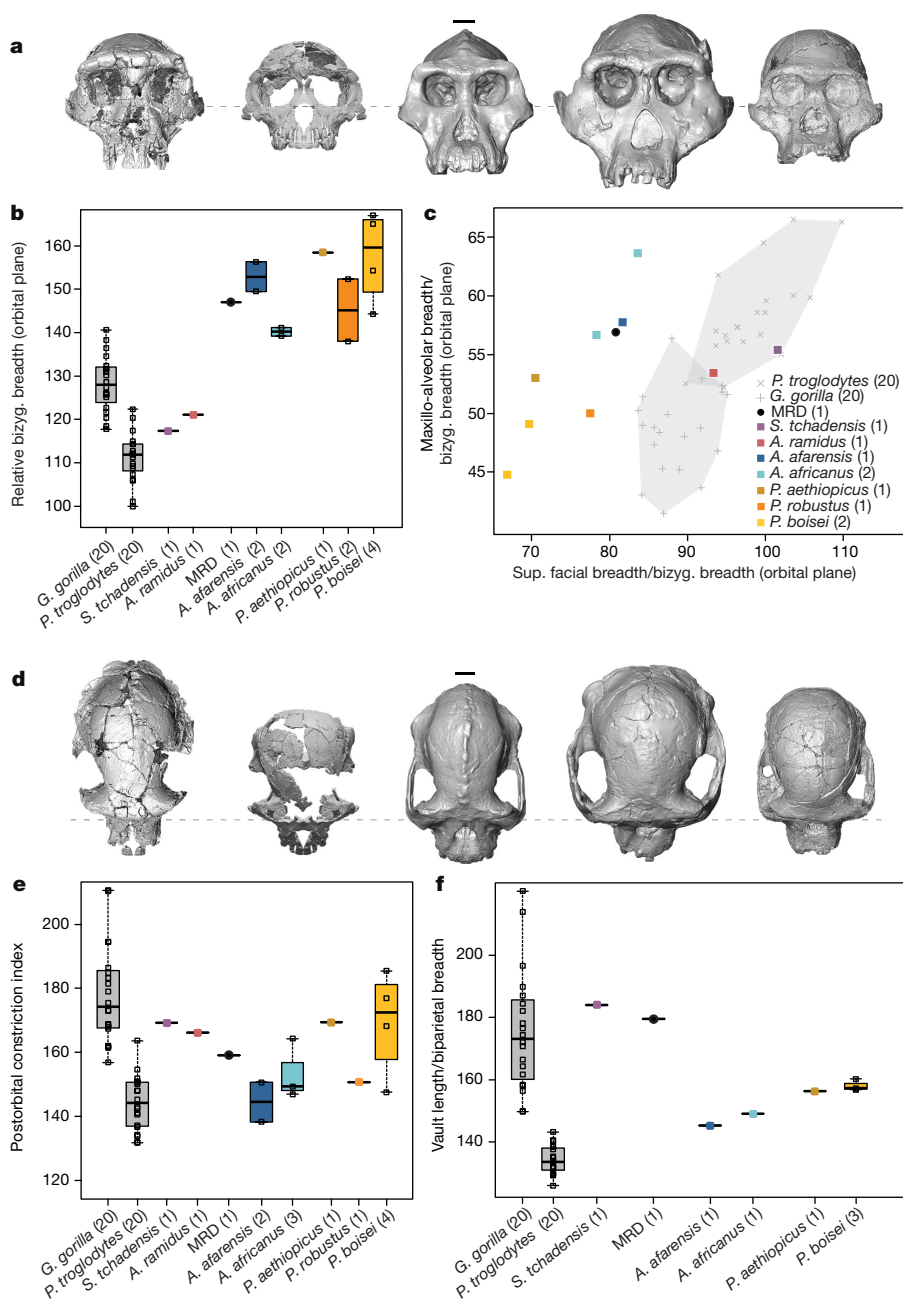
Fig. 3 | Structure of the face and neurocranium. a, Anterior view of early hominin crania. Left to right: *S. tchadensis* (TM 266-01-60-1), composite *A. ramidus* reconstruction, MRD, *A. afarensis* (A.L. 444-2), *A. africanus* (Sts 5). Specimens are oriented in Frankfort horizontal and aligned at orbitale (dashed grey line). **b**, Bizygomatic (bizyg.) breadth (in the orbital plane) relative to biorbital breadth. *G. gorilla, Gorilla gorilla*; *P. aethiopicus, Paranthropus aethiopicus*; *P. boisei, Paranthropus boisei*; *P. troglodytes, Pan troglodytes*. **c**, Bivariate plot of indices that quantify the 'facial mask' shape. **d**, Superior view of early hominin crania (in the same order as in **a**). Specimens are oriented in Frankfort horizontal and aligned at glabella (dashed grey line). **e**, Index of postorbital constriction (superior facial breadth/postorbital constriction). **f**, Index that quantifies the braincase shape. Box plot definitions are as in Fig. 2 and sample sizes are indicated in the figure panels. Scale bars, 2 cm. Images of *A. ramidus* and *S. tchadensis* in **a**, **d** were generated, with permission, from CT scans that have previously been published[26,45].

and falls among the deepest palates of *A. africanus* and *Paranthropus robustus* (Supplementary Note 7).

Analysis of the face

Australopiths share a pattern of facial structure that is characterized by a broad zygomatic region combined with a relatively narrow upper face. This produces an upward-tapering outline (the 'hexagonal facial mask')[27–29]. Although the hexagonal mask is shared among non-robust and robust australopiths, *S. tchadensis*, *A. ramidus* and non-human apes exhibit relatively broader upper faces and lack pronounced zygomatic expansion[26,27]. MRD is similar to other australopiths and distinct from earlier hominins in possessing a broad midface and narrow upper face (Fig. 3a–c). There are facial similarities that are specifically shared between MRD and *A. afarensis*. The external contour of the orbits in MRD and *A. afarensis* is squared off superolaterally and the lateral border of the orbit widens inferiorly. Facial hafting is similar between MRD and non-robust australopiths: the frontal bone is slightly inclined, which positions the face below the braincase, and no post-toral sulcus or frontal trigon is present (Extended Data Fig. 8).

The MRD face is particularly long supero-inferiorly. This morphology stands in stark contrast to the short and gracile face reconstructed for *A. ramidus*. However, comparisons of facial robusticity must consider sexual dimorphism: MRD, A.L. 444-2 and TM 266-01-60-1 probably represent male individuals, whereas the face of the *A. ramidus* composite represents a female[26]. Thus some degree of difference in facial robusticity is expected. The currently available fossil sample does not permit the disentanglement of the morphological differences that are due to sexual dimorphism from those that are taxonomically diagnostic. Furthermore, it has previously been suggested[26] that the short face of the composite reconstruction of *A. ramidus* is not representative of the species. The MRD face is also strongly prognathic, both in the mid-face and subnasally (Extended Data Fig. 8). The projection of the mid-face in MRD is comparable to *S. tchadensis*, but MRD lacks upper facial projection[3,26].

There are some aspects of the MRD face that are reminiscent of *A. africanus* and robust australopiths, and that have traditionally been considered to be derived. The MRD zygomaticoalveolar crest is nearly straight and rises steeply from the alveolar margin. As a result, the

Table 1 | Craniofacial metrics of MRD-VP-1/1 and other early hominins

	MRD-VP-1/1	S. tchadensis TM 266-01-060-1 reconstruction	A. ramidus ARA-VP-6/500 reconstruction	A. afarensis A.L. 444-2	A. africanus Sts 5	Sts 71	Stw 505
Cranial dimensions							
Vault length (g–op)	149.2	173	–	167	146	129	–
Maximum cranial length (pr–op)	205.0	211	162.5 ± 3	215	181	164	–
ba–b height	94.9	86	79.5		101	–	–
Biparietal breadth[a]	83.1	90[p]	91–92.5[j]	115	98	–	–
Maximum cranial breadth[b]	116.3	128	110.5	139	108	–	123
Biporion breadth	108.9	114.2[p]	98.5	132	107	105	(126)
Postorbital breadth[c]	61.9[k]	65	62	77	64	56	71
Occipital upper scale arc (l–op)	26.1	–	–	29	39	33	–
Occipital upper scale angle (l–op)	70.1	(63)[p]	–	70	80	–	–
Occipital lower scale arc (op–o)	56.4	–	–	41	31	38	–
Occipital lower scale angle (op–o)	43.1	36	–	25	40	–	–
Nuchal plane length (i–o)	54.1	42.8[p]	–	–	31	38	–
Facial dimensions							
Superior facial breadth (fmt–fmt)	98.5	110	103	(116)	94	(92)	–
Bizygomatic breadth at the orbital plane[d]	122.0	108.3	107.5[j]	142	120	110	–
Bimaxillary breadth (zm–zm)	92 ± 2[l]	–	83.5	–	106	96	–
Maxillo-alveolar breadth	69.5	60	59	82	68	70	–
Superior facial height (n–pr)	91.1[k]	75	61.5 ± 3	100	77	73	91
Vertical facial height[e]	105	99.5[p]	–	113	86	88	110
Malar height (or–zm)	(34)[l]	26	18		26	27	31[m]
Orbitoalveolar height[f]	59.3	46.8[p]	32.5	66	51	47	62
Masseteric height[g]	38	26.8[p]	18.2[j]	32.3	32.1	31	–
ns–pr height	30.7	21.5	–		29	27	29
ns–pr angle	48.9	50	–	39	37	47	50
Index of palate protrusion[h]	69.4	47	53.2[j]	55	68	43	–
Sellion–pr angle	54.7	(60)[p]	52.5[j]	65	53	65	(58)
Sellion–ns angle	58.1	–	–	76	66	72	66
Biorbital breadth[i]	82.8	91[n]	90.5[n]	95	85	79	97[o]
Interorbital breadth (mf–mf)	23.1[k]	23	16.6[j]	19	20	20	18.6
Orbit breadth (mf–ek)	31.5	37.5	37	40[n]	34	34	39
Orbit height	31.3	35	32	39	29	31	37
Nasal aperture breadth[i]	24.1[k]	26	18.5	25	26	25	29
Nasal aperture height (rhi–ns)	38.7[k]	32	–	37	24	24	28
Internal palate length (ol–sta)	73.6[k]	–	–	75	65.3	–	–

Measurements of MRD are taken from the symmetrized reconstruction, or from the original specimen where the concerned region is undistorted (as indicated). Distances are reported in mm. Angles are measured between the concerned chords and Frankfort horizontal planes and reported in degrees. Values in parentheses or with '±' indicate estimated measurements; '–' indicates unavailable data. Comparative data were assembled from previous studies[27–29,42–45] or collected by the authors. Definitions for the osteometric point abbreviations can be found in a previously published study[46].
[a]Definition follows 'maximum parietal breadth' of ref. [43].
[b]Either bimastoid or bisupramastoid, depending on specimen morphology. For MRD, it is bisupramastoid.
[c]Measurement 9(1) of ref. [46] and measurement 21 of ref. [27] were used.
[d]Measurement 52 of ref. [27] was used.
[e]Measurement 53 of ref. [27] was used.
[f]Measurement 58 of ref. [27] was used.
[g]Measurement 59 of ref. [27] was used.
[h]See definition in refs [27,46].
[i]Maximum breadth parallel to Frankfort horizontal plane.
[j]Measurements provided by G. Suwa (personal communication).
[k]Measurement of the original specimen.
[l]The zygomaxillary suture is obliterated. The position of zm was estimated at the medial third of the zygomatic tubercle.
[m]Minimum malar height as described in ref. [43]. This measurement is equivalent to or–zm in some specimens and 1–3 mm less than or–zm in others.
[n]fmo–fmo, typically 1–3 mm less than maximum breadth.
[o]ek–ek.
[p]Measurement provided by F. Guy (personal communication).

anterior origin of the masseter muscle (the zygomatic tubercle) is superiorly positioned and the tubercle faces inferolaterally. The opposite pattern, in which the crest is low and arched, is traditionally considered to be primitive, because it is shared among A. ramidus, A. afarensis and African apes[30,31]. A ratio of the masseteric height relative to the vertical facial height shows that MRD is similar to A. africanus and robust australopiths in exhibiting a high ratio that indicates a relatively superior masseter position. By contrast, S. tchadensis, A. ramidus and A. afarensis share lower values (Supplementary Note 8). The masseter origin is also anteriorly positioned in MRD, similar to robust australopiths (Supplementary Note 8). However, the anterior position is achieved in a unique way. The infra-orbital malar region is concave in MRD, rather

than flat as in *A. afarensis*. This concavity shifts the lateral portion of the zygomatic body (including the tubercle) more anteriorly than the zygomatic root (Fig. 3d). As a result, the central portion of the face is concealed by the zygomatic bones in lateral view, despite the zygomatic root being positioned at M^1 (Extended Data Fig. 8).

Description of the neurocranium
The MRD neurocranium retains a number of primitive features and sutural patterns. It retains the asterionic notch and the squamosal suture is low and only slightly arched. It is anteroposteriorly elongated and narrow across the parietals—an unusual shape that is shared exclusively with *S. tchadensis* (Fig. 3d, f). Our preliminary estimate of the cranial capacity is 365–370 c.c., similar to *S. tchadensis*. This value is smaller than the smallest female individuals of *A. afarensis*[27,32]. The pronounced postorbital constriction (as indicated by large index value) seen in MRD is shared to various degrees by other hominins, including the most-primitive species, *S. tchadensis* and *A. ramidus*. However, *A. afarensis* differs as it has a relatively wider postorbital region (Fig. 3d, e). In MRD, the sagittal crest begins more anteriorly than in the crania of most hominins and continues posteriorly to merge with the nuchal lines.

The temporal squama of MRD is heavily pneumatized and also has a small external acoustic meatus. The *A. anamensis* temporal fragment (KNM-KP 29281B) shares these features. Although the dimensions of the MRD external acoustic meatus cannot be measured precisely owing to damage, the better-preserved left side is approximately 8.0 mm vertically and 8.9 mm anteroposteriorly with an estimated ellipse area of 55.9 mm^2, which is larger than KNM-KP 29281B[7] (40 mm^2). However, the value of MRD falls in the lower range of *A. afarensis*[27] (47.7–109.3 mm^2; mean = 79.7 mm^2; $n = 4$).

A posterior view reveals a bell-shaped outline, a compound temporal-nuchal crest and a 'bare area' morphology that is comparable to *A. afarensis*[27] (Extended Data Fig. 9). The MRD mastoids are inflated, although they are positioned slightly above the cranial base. As a result, the contour of the cranial base is convex, similar to the condition in *Pan* and to some degree to the condition in *A. africanus*, but in contrast to *A. afarensis* (Extended Data Fig. 9). Another primitive feature of the cranial base is the great length of the nuchal plane. In MRD, the nuchal plane length—standardized by bimastoid breadth—is longer than that of TM266-01-60-1 (Table 1).

Taxonomy and phylogenetic relationships
The morphological comparisons presented above indicate that MRD is best attributed to *A. anamensis*. Although most of the similarities between MRD and *A. anamensis* are plesiomorphic, MRD presents many features that distinguish *A. anamensis* from *A. afarensis*: a relatively large and mesiodistally elongated upper canine, a small external acoustic meatus, a rounded lateral nasal margin with contribution from the canine jugum, a relatively narrow palate and an upper canine aligned with the postcanine row. Morphology of the MRD upper canine is particularly important in taxonomic attribution, because it displays features that appear to be apomorphic in *A. anamensis* (basally positioned crown shoulders and pronounced mesiodistal elongation of the crown). The most notable differences between MRD and the previously known *A. anamensis* hypodigm include the greater inclination of the MRD canine and the greater depth of the palate. However, our comparisons of canine inclination indicate that the magnitude of difference between MRD and other *A. anamensis* specimens is consistent with intraspecific variability (Extended Data Fig. 6 and Supplementary Note 6).

Additional plesiomorphic features of *A. anamensis* are revealed for the first time in MRD. The nuchal plane is very long and postorbital constriction is pronounced. The shape of the neurocranium in superior view has notable similarities to that of *S. tchadensis*. However, aspects of the mid- and upper face show clear affinity to *A. afarensis*. The facial mask is hexagonal and the superolateral corner of the orbits is 'squared off' in a distinctive manner. Facial hafting in MRD is similar to the

condition shared between *A. afarensis* and *A. africanus* (that is, inclined frontal lacking a post-toral sulcus).

A. anamensis is consistently recognized as being phylogenetically positioned between *A. ramidus* and *A. afarensis*[7,19,20,25,33,34]. Although this idea has both chronological and morphological support, the anatomical composition of the previously known hypodigm is limited to comparisons of jaws and teeth. Our understanding is thus primarily based on where *A. anamensis* fits with regard to documented trends in canine reduction and the development of masticatory robusticity. The discovery of MRD presents an opportunity to consider the phylogenetic position of *A. anamensis* using craniofacial morphology.

We conducted phylogenetic analyses by augmenting two character matrices published by independent observers[27,33] with data from MRD (Supplementary Notes 9 and Supplementary Table 1). In one iteration of these analyses, MRD was treated as one specimen within the larger *A. anamensis* hypodigm. The resulting cladograms depict *A. anamensis* as the sister taxon to *A. afarensis* and later hominins, thus reinforcing the widely accepted topology (Extended Data Fig. 10a, b). Results are similar when MRD was treated as a separate operational taxonomic unit (Extended Data Fig. 10c–g, Supplementary Note 9 and Supplementary Table 1). Together, these analyses indicate that the phylogenetic position of *A. anamensis* is consistent, even when different anatomical regions are considered (that is, dentognathic and/or craniofacial morphologies) and despite inter-observer differences in character list composition and scoring.

Although the addition of craniofacial observations does not change the accepted topology, it does alter the implied pattern of morphological evolution. *A. anamensis* is generally portrayed as a primitive extension of *A. afarensis*; this idea has been supported by the apparent lack of derived features in the previously known hypodigm[19,35]. However, the craniofacial morphology of MRD suggests that *A. anamensis* possessed a number of derived features, including the presence of topographic relief in the infraorbital region, a superiorly and anteriorly positioned masseter origin, and potentially additional features (Extended Data Fig. 10h, i and Supplementary Note 9). Notably, the presence of pronounced postorbital constriction in MRD and more primitive hominins confirms the previous suggestion that *A. afarensis* is derived in showing reduced postorbital constriction[27,35]. It also further confirms that the 3.9-Myr-old frontal fragment from the Middle Awash, Ethiopia (BEL-VP-1/1)[36,37], is derived with regard to postorbital constriction and thus probably belongs to *A. afarensis*[27,38] (Supplementary Note 10). Together, the secure dating of BEL-VP-1/1 and MRD indicate that *A. afarensis* and *A. anamensis* overlapped in the Afar Triangle for at least 100,000 years.

Discussion
The 3.8-Myr-old cranium from Woranso-Mille elaborates some of the outstanding questions in Pliocene hominin evolution and fills a major gap in the fossil record. The morphologies of the MRD canine, maxilla and temporal region suggest that this specimen represents *A. anamensis*.

The hypothesis that *A. anamensis* and *A. afarensis* constitute a single evolving chronospecies was based on limited apomorphic features in *A. anamensis*, but is mostly due to perceived temporal trends in morphology in four time-successive samples of the two species from Kanapoi, Allia Bay, Laetoli and Hadar[35]. However, the lack of fossil hominins from 3.9–3.7 Myr ago in general and the lack of complete crania of *A. anamensis* in particular have been major impediments to fully test this hypothesis. The addition of MRD to the *A. anamensis* hypodigm changes our understanding of the relationship between the two taxa. With MRD assigned to *A. anamensis*, it indicates that *A. anamensis* can be clearly distinguished from *A. afarensis* such that the latter species may not have been a result of 'phyletic transformation within an unbranched lineage'[35]. Furthermore, the fact that MRD shares some neurocranial and facial morphological features with younger taxa such as *A. africanus* and *Paranthropus*—albeit considered here to be more likely to have been caused by parallel evolution—is worth further

investigation in the future, as it may have considerable bearing on the origin of *A. africanus* and its relationship with *A. afarensis*. More work is also needed to better understand the geology and Pliocene palaeogeography of the Afar region[18] and establish a refined taxonomy of the Woranso-Mille hominins from 3.8 to 3.4 Myr ago.

On the basis of the currently available fossil evidence, it appears that there were at least four time-successive but allopatric *A. anamensis* populations (Woranso-Mille, Allia Bay, Asa Issie and Kanapoi) that showed variable cranial and dentognathic morphology. Although the cranial morphology of *A. anamensis* was poorly known thus far, the 3.8-Myr-old MRD from Woranso-Mille is morphologically similar to the species from Kanapoi and Asa Issie (4.2–4.1 Myr ago). However, it is unlikely that an *A. anamensis* population represented by MRD gave rise to *A. afarensis*, as MRD postdates BEL-VP-1/1, which now appears to be the earliest known representative of *A. afarensis* with an age of approximately 3.9 Myr. Although their taxonomic affinity is still controversial[39], it is possible that the few approximately 4.0-Myr-old teeth from Fejej, Ethiopia, might also belong to *A. afarensis*[40,41]. These observations can be tested with the recovery of crania from Kanapoi, Asa Issie and Allia Bay and further comparisons to MRD. In summary, although MRD and other discoveries from Woranso-Mille do not falsify the proposed ancestor–descendant relationship between *A. anamensis* and *A. afarensis*, they indicate that *A. afarensis* may not have evolved from a single ancestral population. Most importantly, MRD shows that despite the widely accepted hypothesis of anagenesis, *A. afarensis* did not appear as a result of phyletic transformation. It also shows that at least two related hominin species co-existed in eastern Africa around 3.8 Myr ago, further lending support to mid-Pliocene hominin diversity.

Online content

1. Brunet, M. et al. *Australopithecus bahrelghazali*, une nouvelle espèce d'Hominidé ancien de la région de Koro Toro (Tchad). *C. R. Acad. Sci. IIA* **322**, 907–913 (1996).
2. Brunet, M. et al. New material of the earliest hominid from the Upper Miocene of Chad. *Nature* **434**, 752–755 (2005).
3. Brunet, M. et al. A new hominid from the Upper Miocene of Chad, Central Africa. *Nature* **418**, 145–151 (2002).
4. Haile-Selassie, Y. Late Miocene hominids from the Middle Awash, Ethiopia. *Nature* **412**, 178–181 (2001).
5. Haile-Selassie, Y. et al. New species from Ethiopia further expands Middle Pliocene hominin diversity. *Nature* **521**, 483–488 (2015).
6. Haile-Selassie, Y. et al. A new hominin foot from Ethiopia shows multiple Pliocene bipedal adaptations. *Nature* **483**, 565–569 (2012).
7. Leakey, M. G., Feibel, C. S., McDougall, I. & Walker, A. New four-million-year-old hominid species from Kanapoi and Allia Bay, Kenya. *Nature* **376**, 565–571 (1995).
8. Leakey, M. G., Feibel, C. S., McDougall, I., Ward, C. & Walker, A. New specimens and confirmation of an early age for *Australopithecus anamensis*. *Nature* **393**, 62–66 (1998).
9. Leakey, M. G. et al. New hominin genus from eastern Africa shows diverse middle Pliocene lineages. *Nature* **410**, 433–440 (2001).
10. Senut, B. et al. First hominid from the Miocene (Lukeino formation, Kenya). *C. R. Acad. Sci. IIA* **332**, 137–144 (2001).
11. White, T. D., Suwa, G. & Asfaw, B. *Australopithecus ramidus*, a new species of early hominid from Aramis, Ethiopia. *Nature* **371**, 306–312 (1994).
12. White, T. D. et al. *Ardipithecus ramidus* and the paleobiology of early hominids. *Science* **326**, 64–86 (2009).
13. Wood, B. & K Boyle, E. Hominin taxic diversity: fact or fantasy? *Am. J. Phys. Anthropol.* **159**, 37–78 (2016).
14. Haile-Selassie, Y., Melillo, S. M. & Su, D. F. The Pliocene hominin diversity conundrum: do more fossils mean less clarity? *Proc. Natl Acad. Sci. USA* **113**, 6364–6371 (2016).
15. Haile-Selassie, Y. et al. Dentognathic remains of *Australopithecus afarensis* from Nefuraytu (Woranso-Mille, Ethiopia): comparative description, geology, and paleoecological context. *J. Hum. Evol.* **100**, 35–53 (2016).
16. Haile-Selassie, Y. Phylogeny of early *Australopithecus*: new fossil evidence from the Woranso-Mille (central Afar, Ethiopia). *Phil. Trans. R. Soc. Lond. B* **365**, 3323–3331 (2010).
17. Haile-Selassie, Y., Saylor, B. Z., Deino, A., Alene, M. & Latimer, B. M. New hominid fossils from Woranso-Mille (Central Afar, Ethiopia) and taxonomy of early *Australopithecus*. *Am. J. Phys. Anthropol.* **141**, 406–417 (2010).
18. Saylor, B. Z. et al. Age and context of new mid-Pliocene hominin cranium from Woranso-Mille, Ethiopia. *Nature* https://doi.org/10.1038/s41586-019-1514-7 (2019).
19. Ward, C. V., Leakey, M. G. & Walker, A. Morphology of *Australopithecus anamensis* from Kanapoi and Allia Bay, Kenya. *J. Hum. Evol.* **41**, 255–368 (2001).
20. Ward, C. V., Manthi, F. K. & Plavcan, J. M. New fossils of *Australopithecus anamensis* from Kanapoi, West Turkana, Kenya (2003–2008). *J. Hum. Evol.* **65**, 501–524 (2013).
21. Ward, C. V., Plavcan, J. M. & Manthi, F. K. New fossils of *Australopithecus anamensis* from Kanapoi, West Turkana, Kenya (2012–2015). *J. Hum. Evol.* https://doi.org/10.1016/j.jhevol.2017.07.008 (2017).
22. Manthi, F. K., Plavcan, J. M. & Ward, C. V. New hominin fossils from Kanapoi, Kenya, and the mosaic evolution of canine teeth in early hominins. *S. Afr. J. Sci.* **108**, 724 (2012).
23. Suwa, G. et al. Paleobiological implications of the *Ardipithecus ramidus* dentition. *Science* **326**, 69–99 (2009).
24. Haile-Selassie, Y., Suwa, G. & White, T. D. Late Miocene teeth from Middle Awash, Ethiopia, and early hominid dental evolution. *Science* **303**, 1503–1505 (2004).
25. White, T. D. et al. Asa Issie, Aramis and the origin of *Australopithecus*. *Nature* **440**, 883–889 (2006).
26. Suwa, G. et al. The *Ardipithecus ramidus* skull and its implications for hominid origins. *Science* **326**, 68–68e7 (2009).
27. Kimbel, W. H., Rak, Y. & Johanson, D. C. *The Skull of Australopithecus afarensis* (Oxford Univ. Press, 2004).
28. Guy, F. et al. Morphological affinities of the *Sahelanthropus tchadensis* (Late Miocene hominid from Chad) cranium. *Proc. Natl Acad. Sci. USA* **102**, 18836–18841 (2005).
29. Rak, Y. *The Australopithecine Face* (Academic, 1983).
30. Kimbel, W. H. & Rak, Y. *Australopithecus sediba* and the emergence of *Homo*: Questionable evidence from the cranium of the juvenile holotype MH 1. *J. Hum. Evol.* **107**, 94–106 (2017).
31. Kimbel, W. H., White, T. D. & Johanson, D. C. Cranial morphology of *Australopithecus afarensis*: a comparative study based on a composite reconstruction of the adult skull. *Am. J. Phys. Anthropol.* **64**, 337–388 (1984).
32. Kimbel, W. H. & Rak, Y. The cranial base of *Australopithecus afarensis*: new insights from the female skull. *Phil. Trans. R. Soc. Lond. B* **365**, 3365–3376 (2010).
33. Strait, D. S. & Grine, F. E. Inferring hominoid and early hominid phylogeny using craniodental characters: the role of fossil taxa. *J. Hum. Evol.* **47**, 399–452 (2004).
34. Dembo, M., Matzke, N. J., Mooers, A. Ø. & Collard, M. Bayesian analysis of a morphological supermatrix sheds light on controversial fossil hominin relationships. *Proc. R. Soc. Lond. B* **282**, 20150943 (2015).
35. Kimbel, W. H. et al. Was *Australopithecus anamensis* ancestral to *A. afarensis*? A case of anagenesis in the hominin fossil record. *J. Hum. Evol.* **51**, 134–152 (2006).
36. Asfaw, B. The Belohdelie frontal: new evidence of early hominid cranial morphology from the Afar of Ethiopia. *J. Hum. Evol.* **16**, 611–624 (1987).
37. Renne, P. R. et al. Chronostratigraphy of Mio-Pliocene Sagantole Formation, Middle Awash Valley, Afar rift, Ethiopia. *Bull. Geol. Soc. Am.* **111**, 869–885 (1999).
38. Kimbel, W. H., Johanson, D. C. & Rak, Y. The first skull and other new discoveries of *Australopithecus afarensis* at Hadar, Ethiopia. *Nature* **368**, 449–451 (1994).
39. Ward, C. V. Taxonomic affinity of the Pliocene hominin fossils from Fejej, Ethiopia. *J. Hum. Evol.* **73**, 98–102 (2014).
40. Fleagle, J. G., Rasmussen, D. T., Yirga, S., Bown, T. M. & Grine, F. E. New hominid fossils from Fejej, Southern Ethiopia. *J. Hum. Evol.* **21**, 145–152 (1991).
41. Kappelman, J. et al. Age of *Australopithecus afarensis* from Fejej, Ethiopia. *J. Hum. Evol.* **30**, 139–146 (1996).
42. Kimbel, W. H., Johanson, D. C. & Coppens, Y. Pliocene hominid cranial remains from the Hadar Formation, Ethiopia. *Am. J. Phys. Anthropol.* **57**, 453–499 (1982).
43. Wood, B. *Koobi Fora Research Project: Hominid Cranial Remains* Vol. 4 (Clarendon, 1991).
44. Lockwood, C. A. & Tobias, P. V. A large male hominin cranium from Sterkfontein, South Africa, and the status of *Australopithecus africanus*. *J. Hum. Evol.* **36**, 637–685 (1999).
45. Zollikofer, C. P. et al. Virtual cranial reconstruction of *Sahelanthropus tchadensis*. *Nature* 434, 755–759 (2005).
46. Martin, R. & Knussman, R. *Anthropologie: Handbuch der vergleichenden Biologie des Menschen* Vol. 1 (Gustav Fischer, 1988).

METHODS

Computed tomography. The MRD cranium was scanned using a GE v|tome|x L300 industrial multiscale microcomputed tomography scanner at the Pennsylvania State University Center for Quantitative Imaging. The cranium was scanned with source energy settings of 180 kV and 420 μA, 0.2-mm Al filter, 2,400 projections, 5 frames averaged per projection and a detector timing of 500 ms. The data were reconstructed with an isotropic voxel size of 75 μm. The data were segmented and a three-dimensional isosurface of the external surface of the fossil was created in Avizo v.9.3 (ThermoFisher Scientific).

Reconstruction of the MRD cranium. Reconstruction of MRD involved reconstructing the facial skeleton and neurocranium, integrating missing parts, reconstructing the endocast and estimating cranial capacity. These procedures are described below.

Digital reconstruction of the facial skeleton. The surface obtained was divided into neurocranial (endocranium and ectocranium) and facial portions. In the original fossil, these two parts were glued together, but this intervention resulted in a mismatch between neurocranium and face, in which the facial portion is medially distorted on the left side. The misalignment appears more evident when the midsagittal plane is computed for the neurocranium (using a best-fit plane for glabella, nasion, sagittal crest and median nuchal line) and the facial portion (using a best-fit plane for rhinion, anterior nasal spine, incisive foramen and points selected on the maxillary suture). The angle computed between the two planes is 6.2° (Extended Data Fig. 1a). The facial portion was rotated to align the midsagittal plane of the face with the midsagittal plane of the neurocranium[47]. Then, the facial portion was moved along the midsagittal plane (that is, upward/downward, forward/backward) once the alignment with the neurocranium was established (Extended Data Fig. 1b). Distorted and missing regions were restored first by mirroring the contralateral unaffected portions of the facial bones, by then using an iterative closest-point algorithm to enhance the alignment between mirrored and original homologous regions and finally by cropping and merging the reconstructed parts to the original preserved portions of MRD. Small gaps were closed using surface interpolation, maintaining—where possible—the original features of the fossil. Specifically, the left supraorbital and zygomatic bones were mirrored to reconstruct missing regions on the right side (Extended Data Fig. 1c). Then, the reconstructed right hemiface was mirrored and aligned with the left part, thus restoring the deformation of the maxilla (Extended Data Fig. 1d). Because most of the left upper teeth are preserved in the original, the mirrored right maxilla was used to correctly realign the original left maxillary dental arcade and part of the palate, thus preserving the original features of the fossil (Extended Data Fig. 1e, f). Finally, because only the third molar (M^3) is preserved on the right side, the left dental arcade (except the right M^3) was reconstructed by mirroring the left counterpart (Extended Data Fig. 1g, h). All of the procedures described above were performed in Geomagic Design X (3D Systems Software)[48,49].

Symmetrization. A template consisting of 47 landmarks and 707 semilandmarks (217 curve semilandmarks and 490 surface semilandmarks) was created on the MRD cranium in Viewbox software (dHAL Software) to capture the geometry of the cranial surface (Extended Data Fig. 2a, b and Supplementary Note 2). The MRD digital model was mirrored along its midsagittal plane to create a complete, symmetric (semi)landmark configuration. The paired landmarks were reflected/relabelled (Extended Data Fig. 2c, d) whereas the semilandmarks were allowed to slide to reduce the bending energy with respect to the original configuration. Then, both configurations were superimposed using a generalized Procrustes analysis, and the Procrustes average (consensus) shape (which is symmetrical by definition) was computed[47–49]. Procrustes coordinates of the symmetric configuration were transformed to Cartesian coordinates by multiplying each (semi)landmark by the centroid size mean (the mean between the centroid size of the two configurations). Finally, the original MRD (semi)landmark configuration was warped into the symmetric (semi)landmark configuration using the thin plate spline (TPS) interpolation functions[42] in Avizo. The surface of the MRD digital model was warped so as to minimize the bending energy of the according transformation (Extended Data Fig. 2e).

Reconstruction of the neurocranium. Further reconstruction of the neurocranium entailed creating a mirror-image copy followed by iterative closest-point superimposition of undistorted regions in order to reconstruct the right temporal process of the zygomatic arch, the left mastoid process and other incomplete parts of the basicranium (Extended Data Fig. 2f–h). We use 'MRD-sym' to refer to the surface model that results from the procedures described above (facial reconstruction, mirror imaging and symmetrization). MRD-sym was produced exclusively using data present in the original specimen.

Integration of missing parts. The rest of missing or incomplete regions of MRD-sym (specifically, the orbital cavities, the zygomatic arches, the sphenoid bone, the foramen magnum and portions of the endocranium) were restored with reference to morphology present in other hominin crania. Reference (semi)landmark configurations were created in Viewbox software on the crania of three different

hominins (reference templates): Sts 5 (*A. africanus* = 650 (semi)landmarks (Extended Data Fig. 3a, b and Supplementary Note 3)), A.L. 444-2 (*A. afarensis* = 438 (semi)landmarks (Extended Data Fig. 4a, b and Supplementary Note 4)) and KNM-WT 17000 (*P. aethiopicus* = 312 (semi)landmarks (Extended Data Fig. 4e, f and Supplementary Note 5)). First, the Sts 5 reference template was applied to MRD-sym to reconstruct the orbital cavities, the sphenoid bone, the foramen magnum and portions of the endocranium, as well as the zygomatic arch and small portions of the frontal process of the zygomatic bone. Semilandmarks were allowed to slide along curves and surfaces to minimize the bending energy of the TPS interpolation computed between the target and each reference, and the semilandmarks that fell in the missing regions were allowed to move without constraints (Extended Data Fig. 3c). The (semi)landmarks of the reference template were thus transformed into the corresponding (semi)landmarks of the target using the TPS functions[50], whereas the surface of the reference was interpolated to minimize the bending energy of the relative transformation (Extended Data Fig. 3d). The corresponding areas of the missing regions of interest were isolated from the resulting warped surface and merged with the three-dimensional MRD-sym model (Extended Data Fig. 3e–h). We use 'MRD-Sts 5' to refer to the surface model that results from using Sts 5 as a reference specimen to integrate the missing parts. The (semi)landmark configurations created on A.L. 444-2 (Extended Data Fig. 4a, b) and KNM-WT 17000 (Extended Data Fig. 4e, f) were similarly applied to MRD-sym (Extended Data Fig. 4c, g) to create alternative reconstructions of the zygomatic arch and the frontal process of the zygomatic bone, following the same methodological procedures described above (Extended Data Fig. 4d, h). Because warping reference hominin crania might introduce slight asymmetries in the reconstructed regions, and because for *P. aethiopicus* only the left side was available to reconstruct the zygomatic arch, the left hemi-cranium of MRD-sym was mirrored along the midsagittal plane to replace the right counterpart. Care was taken to preserve the sagittal and nuchal crests of MRD-sym. The names 'MRD-A.L. 444-2' and 'MRD-WT 17000' refer to the alternative reconstructions using these specimens as references.

Reconstruction of the endocast and estimation of cranial capacity. To estimate cranial capacity, the endocast was segmented manually in Avizo v.9.3. The poor greyscale contrast between the fossil and the matrix infill necessitated manual tracing of the internal endocranial bone surface. For this reconstruction, only the right half of the endocranium was used, owing to the distortion on the left side of the cranium. The hemi-endocast was then mirrored and aligned to produce a complete, undistorted and symmetrical reconstruction.

Phylogenetic analyses. Parsimony analyses were conducted using a branch and bound search algorithm. Character ordering, weighting and outgroup treatment followed the methods described in the original publications[27,33]. We report standard descriptors associated with parsimony analyses, including the tree length, consistency index and retention index.

We analysed the character matrices in multiple iterations, in which MRD was treated either as its own operational taxonomic unit (OTU) or as one specimen within the larger *A. anamensis* hypodigm. Our scorings for MRD and any alterations to published matrices are described in Supplementary Table 1. Strait and Grine[33] included an *A. anamensis* OTU based on the Kenyan specimens known before 2004. Thus, in one iteration of the Strait and Grine character matrix (hereafter, S&G-separate) there is a 'pre-2004 *A. anamensis*' OTU that is composed of specimens that could be scored for dentognathic characters but not for most cranial characters. We added a separate OTU for MRD, which could be scored for cranial characters but not for most dental and mandibular characters. In another iteration (S&G-combined), the samples are combined into a single 'MRD-*A. anamensis*' OTU. With regard to the few characters that could be scored for both the pre-2004 *A. anamensis* and MRD samples, the scorings were either consistent between samples or could be accommodated by a pre-existing category of 'variable' (used to represent a polymorphic population). We conducted comparable analyses using the matrix of Kimbel et al.[27]—one iteration treating MRD as its own taxonomic unit (K-separate) and the second combining MRD and previously attributed *A. anamensis* specimens (K-combined). Because the previous analysis[27] did not include *A. anamensis*, our scorings for *A. anamensis* in the K-combined matrix are based on first-hand comparison of the original fossils, together with published descriptions and comparative data.

The varied OTU treatment of MRD and other specimens attributed to *A. anamensis* allows the phylogenetic placement of MRD to be assessed with or without the assumptions implied by our species attribution. Our alpha taxonomic designation is embedded in the K-combined and S&G-combined analyses—the MRD cranial features are associated with the dentognathic features of the pre-2004 *A. anamensis* sample and any differences between the samples are taken to represent intraspecific polymorphism. By contrast, these assumptions are avoided in the K-separate and S&G-separate analyses, in which MRD can be understood as a separate site sample, a subspecies or as a different species. Assuming that the conspecific designation is correct, the OTU separation further permits us to assess

whether different character subsets (for example, cranial versus dentognathic) convey consistent information about the phylogenetic placement of *A. anamensis*.
Reporting summary. Further information on research design is available in the Nature Research Reporting Summary linked to this paper.

Data availability
The data that support the findings of this study that were not included in the Supplementary Information are available from the corresponding authors upon reasonable request.

47. Benazzi, S., Gruppioni, G., Strait, D. S. & Hublin, J.-J. Technical note: virtual reconstruction of KNM-ER 1813 *Homo habilis* cranium. *Am. J. Phys. Anthropol.* **153**, 154–160 (2014).
48. Besl, P. J. & McKay, N. D. A method for registration of 3-D shapes. *IEEE Trans. Pattern Anal. Mach. Intell.* **14**, 239–256 (1992).
49. Zhang, Z. Iterative point matching for registration of free-form curves and surfaces. *Int. J. Comput. Vis.* **13**, 119–152 (1994).
50. Bookstein, F. L. *Morphometric Tools for Landmark Data: Geometry and Biology* (Cambridge Univ. Press, 1997).

Author contributions Y.H.-S. and S.M.M. conducted fieldwork and collected data. T.M.R. scanned the specimen using computed tomography. T.M.R., S.B. and A.V. performed the three-dimensional reconstruction with contributions from Y.H.-S. and S.M.M. Y.H.-S. and S.M.M. performed the comparative analysis. S.M.M. and Y.H.-S. wrote the paper with contributions from T.M.R., S.B. and A.V.
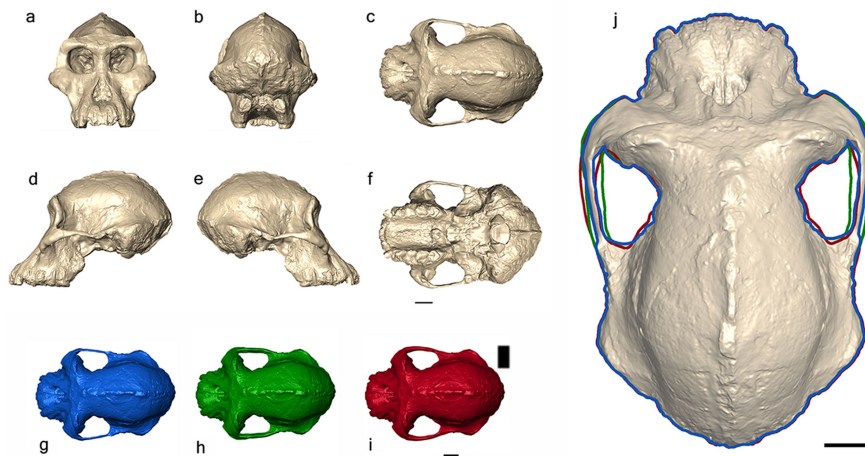
**Extended Data Fig. 1 | MRD-VP-1/1 digital reconstructions.** Digitally reconstructed cranium and comparison of three alternative reconstructions. **a–f**, The reconstructed cranium MRD- Sts 5 is shown in anterior view (**a**), posterior view (**b**), superior view (**c**), left (**d**) and right (**e**) lateral views and inferior view (**f**). Additional images illustrate minor differences in reconstructed zygomatic arches. **g**, MRD-Sts 5. **h**, MRD-A.L. 444-2. **i**, MRD-WT 17000. **j**, MRD-Sts 5 with edges superimposed to the three different restored versions: MRD-Sts 5 (blue lines); MRD-A.L. 444-2 (green lines) and MRD-WT 17000 (red lines). Scale bars, 2 cm.
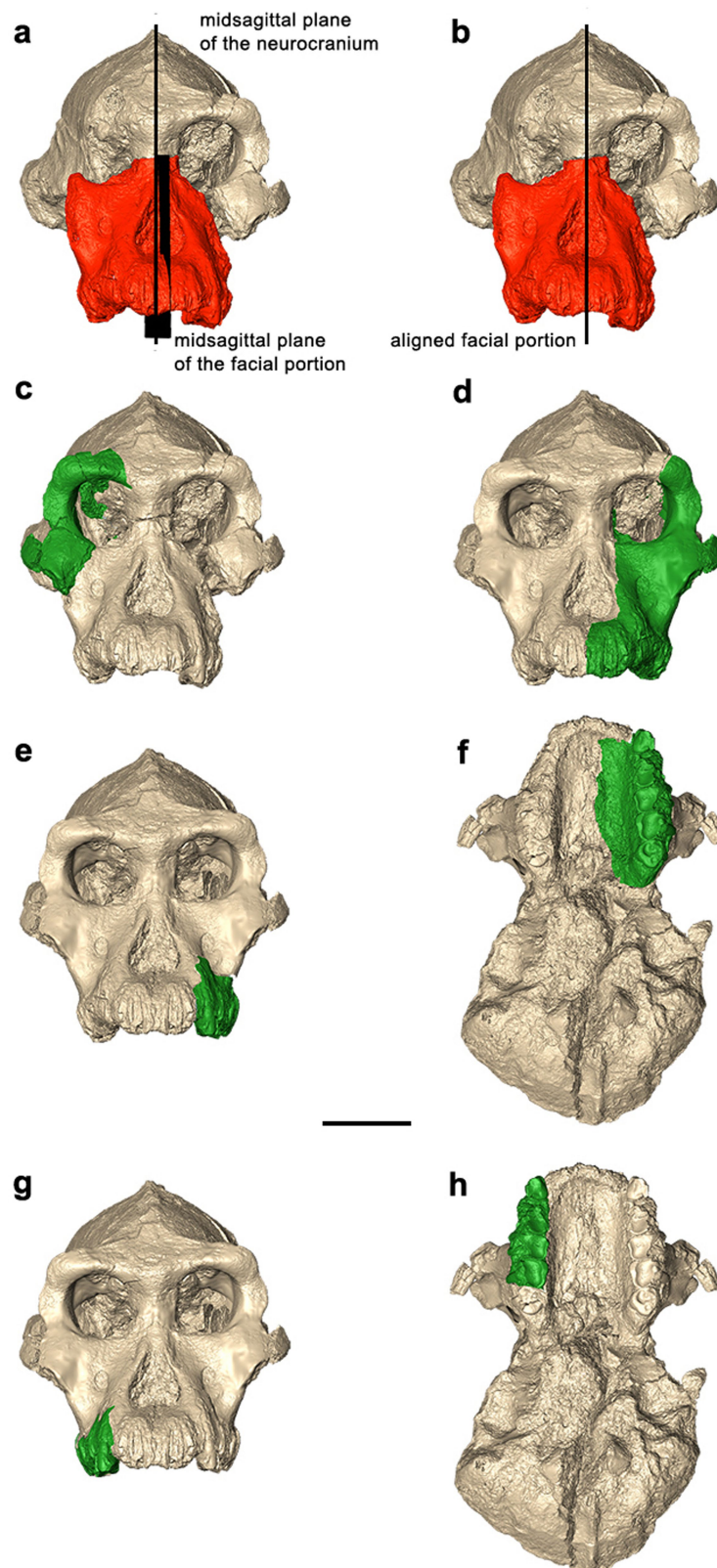
Extended Data Fig. 2 | Basic steps involved in repositioning and reconstructing the MRD face. a, Midsagittal planes computed for the original neurocranium (ivory) and facial portion (red). **b**, The original facial portion is rotated to align the midsagittal plane of the face with the midsagittal plane of the neurocranium, then the former is moved along the midsagittal plane to establish contact with the latter. **c**, The left supra-orbital bone was mirrored and aligned to the original MRD right side. **d**, The complete right side was mirrored and aligned to the left side. **e**, **f**, Anterior (**e**) and inferior (**f**) views of the original left maxillary dental arcade and part of the palate superimposed to the mirrored copy of the right hemiface. **g**, **h**, Frontal (**g**) and basal (**h**) view of the right dental arcade reconstructed by mirroring the left dental arcade (except for the right M^3). Mirrored portions are shown in green. Scale bar, 4 cm. See Methods for details.
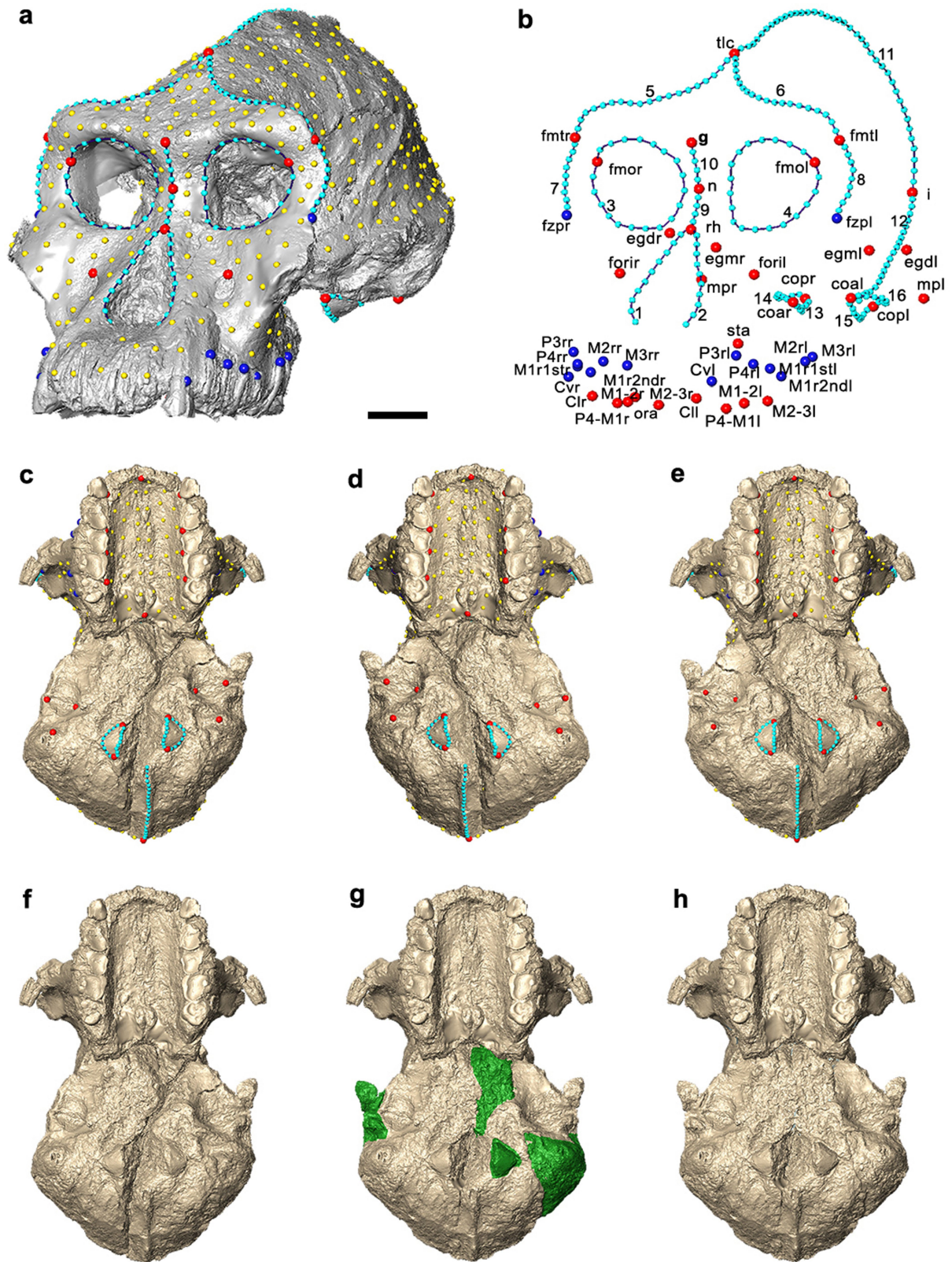
Extended Data Fig. 3 | MRD symmetrization using a reflected relabelling procedure and neurocranium reconstruction. a, The template with landmarks (red), non-osteometric homologous landmarks (blue), curve semilandmarks (light blue) and surface semilandmarks (yellow) was digitized on the MRD cranium. **b**, The template configuration with names of landmarks and curves numbers (Supplementary Note 2). **c**, Basal view of the template digitized on the MRD cranium. **d**, The template digitized on the mirrored cranium. **e**, Symmetric configuration of the (semi)landmarks and warped surface. **f**, Basal view of the final result for MRD-sym. **g**, Basal view of the left zygomatic process, the right mastoid process and other parts of the basicranium reconstructed by mirroring the original counterparts (integrated parts are shown in green). **h**, Basal view, final result after integrating the mirrored counterparts. Scale bars, 2 cm. See Methods for details.
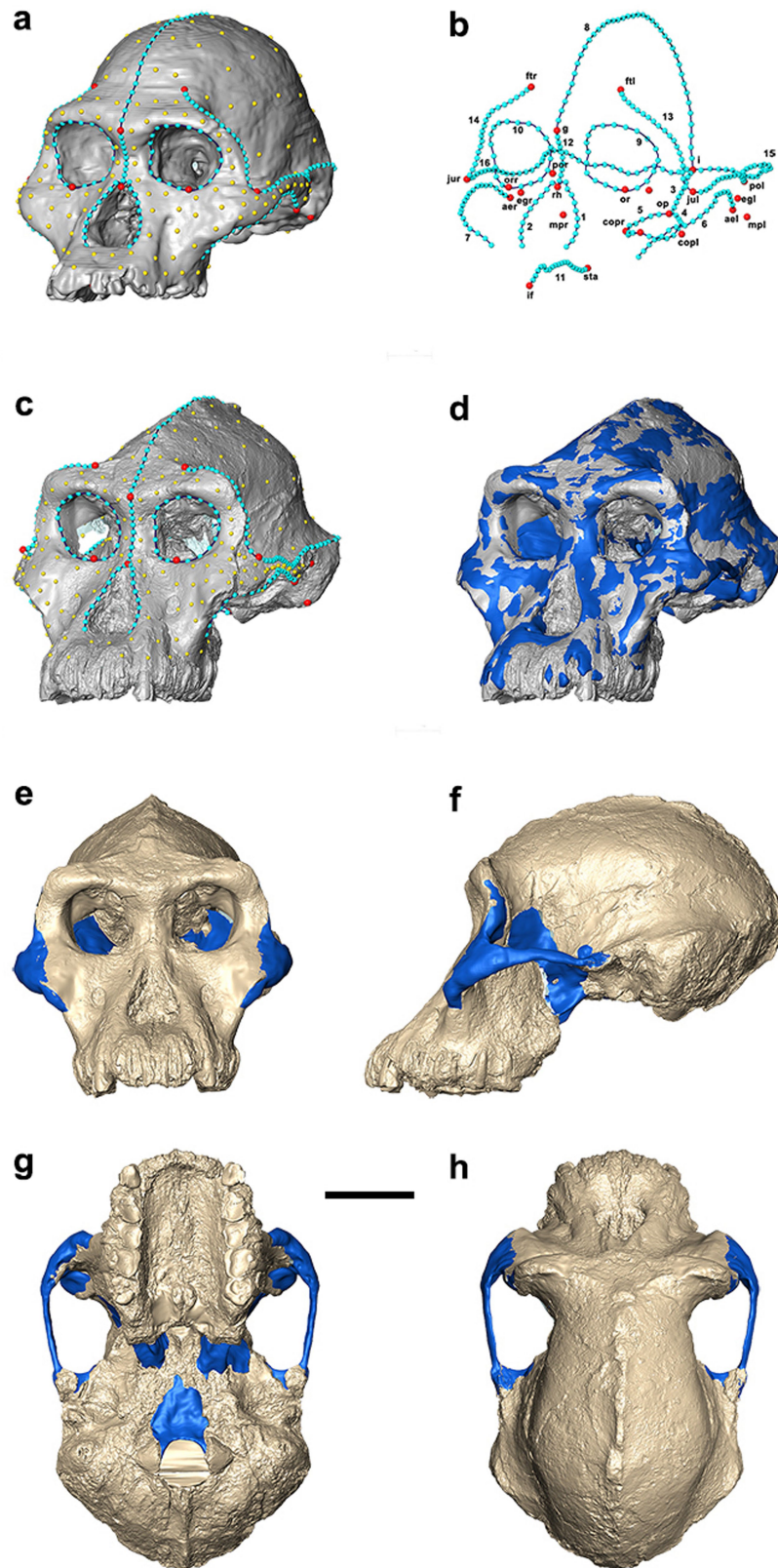
Extended Data Fig. 4 | Integration of missing parts using Sts 5.
a, Template built on the cranium of *A. africanus* (Sts 5). Templates with landmarks (red), curve semilandmarks (light blue) and surface semilandmarks (yellow) were digitized on Sts 5. **b**, Template configuration with names of landmarks and curves numbers (labels are related to Supplementary Note 3). **c**, The same set of (semi)landmarks on the MRD-sym cranium. **d**, TPS interpolation of the Sts 5 cranium, warped to MRD-sym (blue and grey, respectively). **e**–**h**, MRD-sym with the integrated missing parts (blue) isolated from the resulting warped surfaces obtained by the deformation of Sts 5 (shown here as an example) in anterior (**e**), left lateral (**f**), inferior (**g**) and superior (**h**) views. Scale bar, 4 cm.
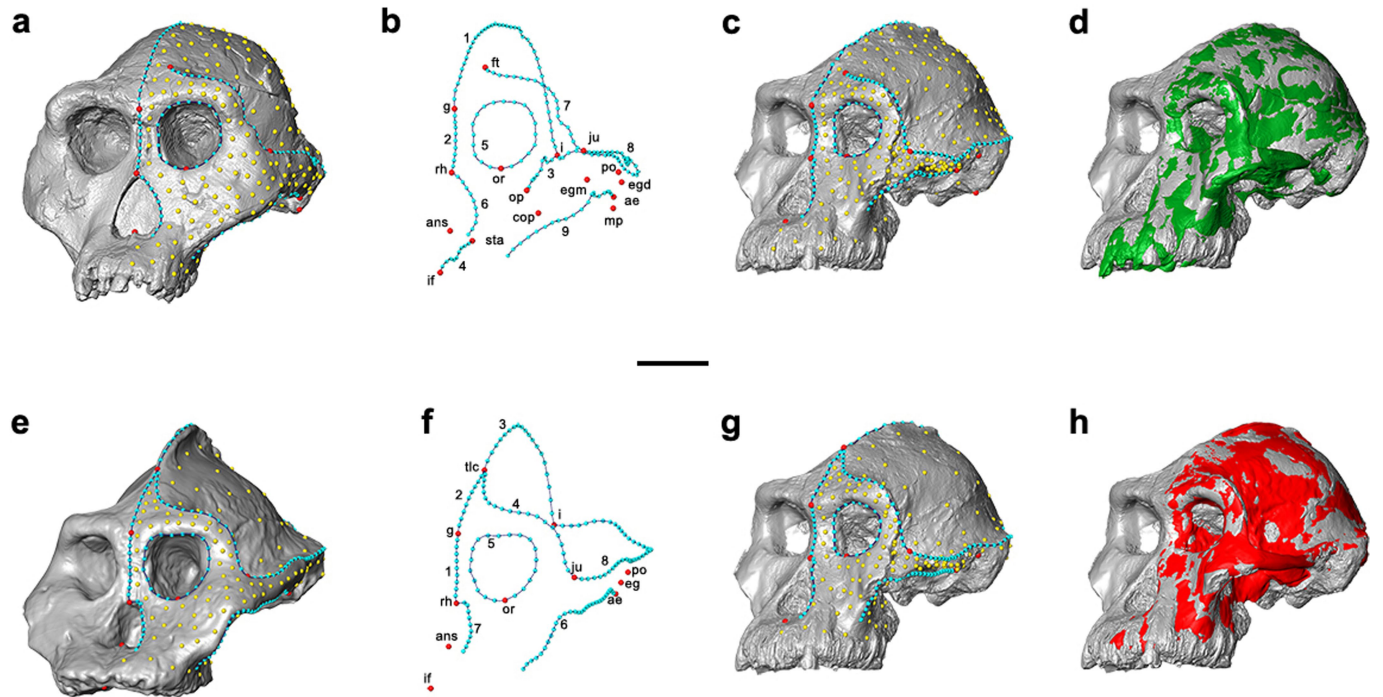
Extended Data Fig. 5 | Integration of missing parts using A.L. 444-2 and KNM-WT 17000. a, **e**, Templates with landmarks (red), curve semilandmarks (light blue) and surface semilandmarks (yellow) digitized on A.L. 444-2 (**a**) and KNM-WT 17000 (**e**) crania. **b**, **f**, The configurations of (semi)landmarks with names of landmarks and curves numbers digitized on A.L. 444-2 (**b**) and KNM-WT 17000 (**f**) crania (labels are related to Supplementary Notes 4, 5). **c**, **g**, Sets of (semi)landmarks on the MRD-sym cranium. **d**, **h**, TPS interpolation of the A.L. 444-2 (green) and KMN-WT 17000 (red) crania warped to MRD-sym (grey). Scale bar, 4 cm.
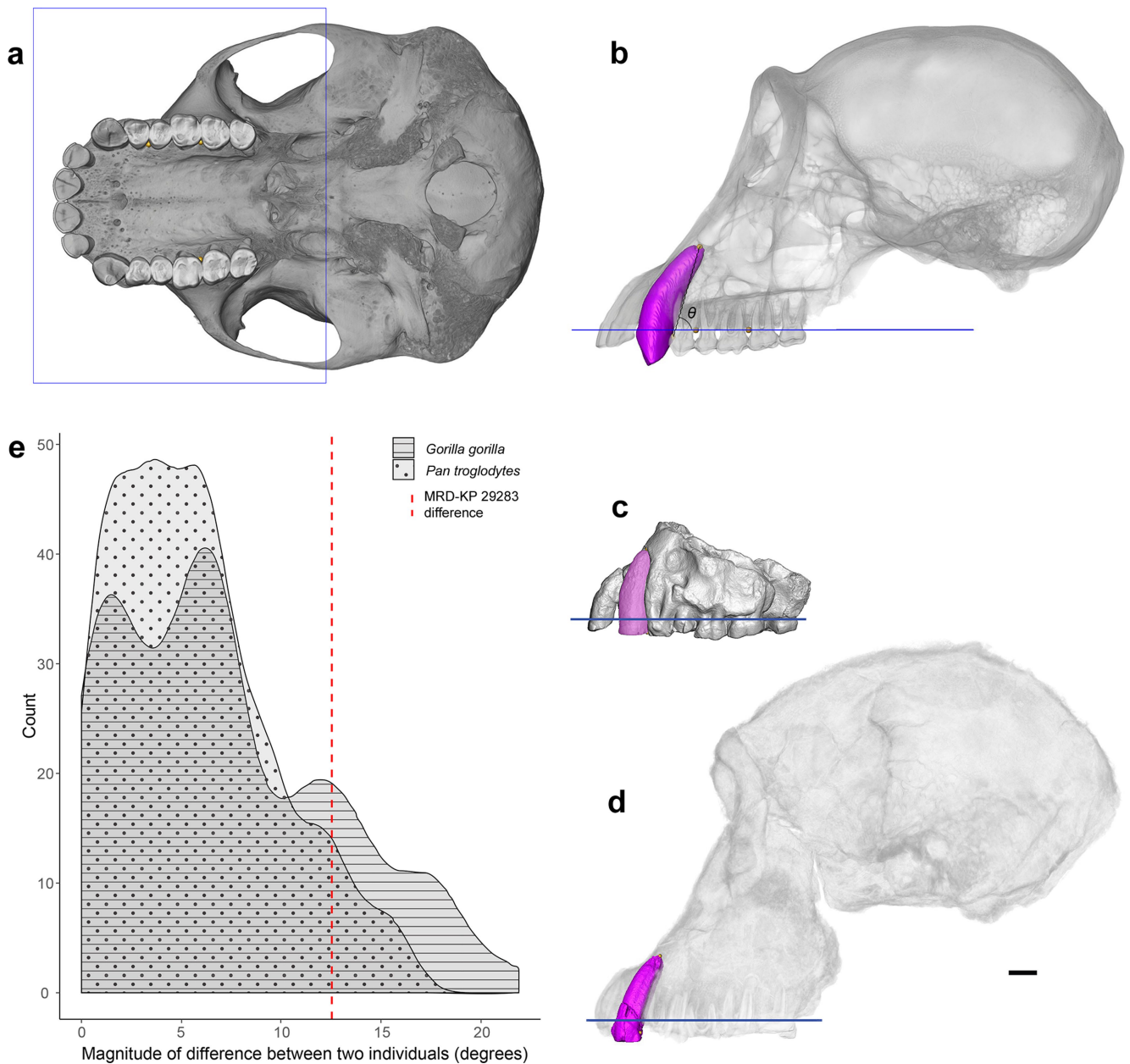
Extended Data Fig. 6 | Canine orientation in MRD and KNM-KP 29283.
The method for measuring the implantation angle of the upper canine
is shown in **a**, **b**. **a**, The internal alveolar plane was established by best-
fitting a plane (outlined in blue) to three landmarks between left P³ and
P⁴, between right P³ and P⁴ and between left M¹ and M². **b**, Landmarks
were placed at the root tip and at the occlusal-most incursion along the
distal enamel line. Upper canine implantation was measured in lateral
view as the two-dimensional angle (θ) between a line connecting the
canine landmarks and the axis of the alveolar plane. **c**, **d**, Upper canine
implantation in the fossil specimens. **c**, *A. anamensis* paratype maxilla
KNM-KP 29283. **d**, MRD. Of the other two *A. anamensis* maxillae

currently known, one (KNM-KP 58579) is qualitatively similar to
KNM-KP 29283 and the other (ARA-VP-14/1) is more inclined. Scale
bar, 1 cm. The scale bar applies to images in **c** and **d**. **e**, The magnitude
of difference in canine implantation angle between MRD and KNM-KP
29283 (12.5°, red dashed line) is shown in the context of expected
conspecific differences. The expectation distributions were constructed
using a permutation approach, for which the measurements from
two individuals were randomly drawn (without replacement) from a
comparative sample and the difference in orientation angle was computed.
This procedure was repeated 500 times, separately for comparative species
*P. troglodytes* and *G. gorilla* (Supplementary Note 6.2).

A. afarensis

A. anamensis

A.L. 199-1

KNM-ER 30745

MRD-VP-1/1

A.L. 444-2

KNM-KP 29283
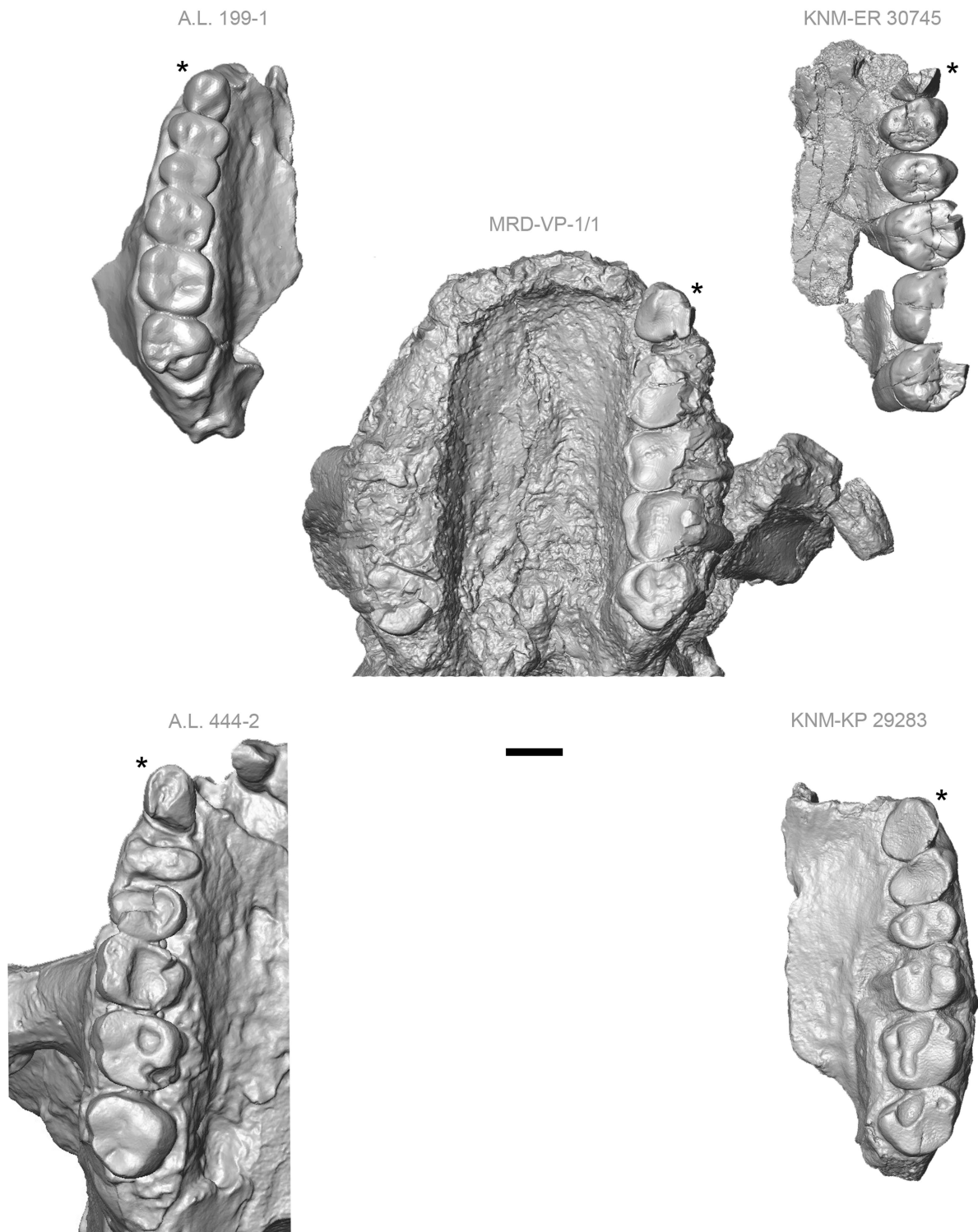
Extended Data Fig. 7 | Maxillary arcade shape. Maxillae in occlusal view of select *A. afarensis* and *A. anamensis* specimens and MRD (original, as preserved). The canine and postcanine teeth form a nearly straight line in *A. anamensis* and MRD. By contrast, the canine tends to be slightly medially offset relative to the postcanine row in many *A. afarensis* specimens. The position of the canine is indicated by the black asterisk. Scale bar, 1 cm.
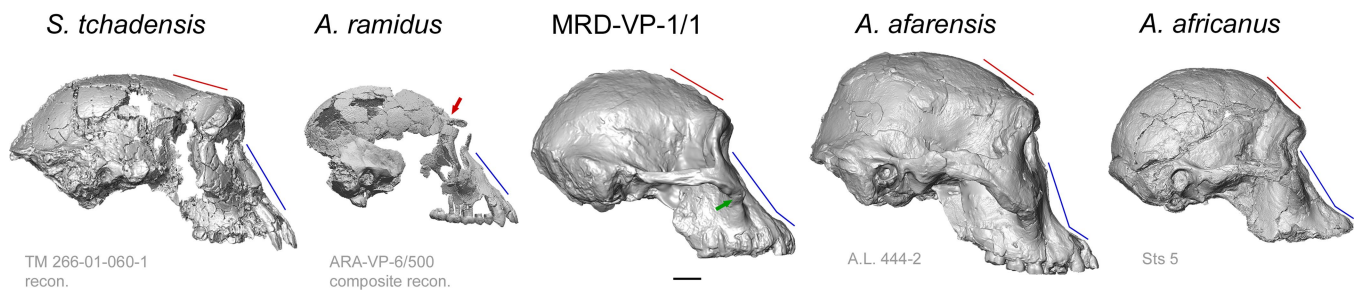
Extended Data Fig. 8 | Comparison of crania in lateral view. Red lines and arrows show the inclination of the frontal and the presence of a post-toral sulcus, respectively. Blue lines show the orientation of the mid and lower face, with an broken line indicating a segmented facial profile[27]. The green arrow marks the anterior projection of the zygomatic tubercle (relative to the anterior zygomatic root). Scale bar, 2 cm.
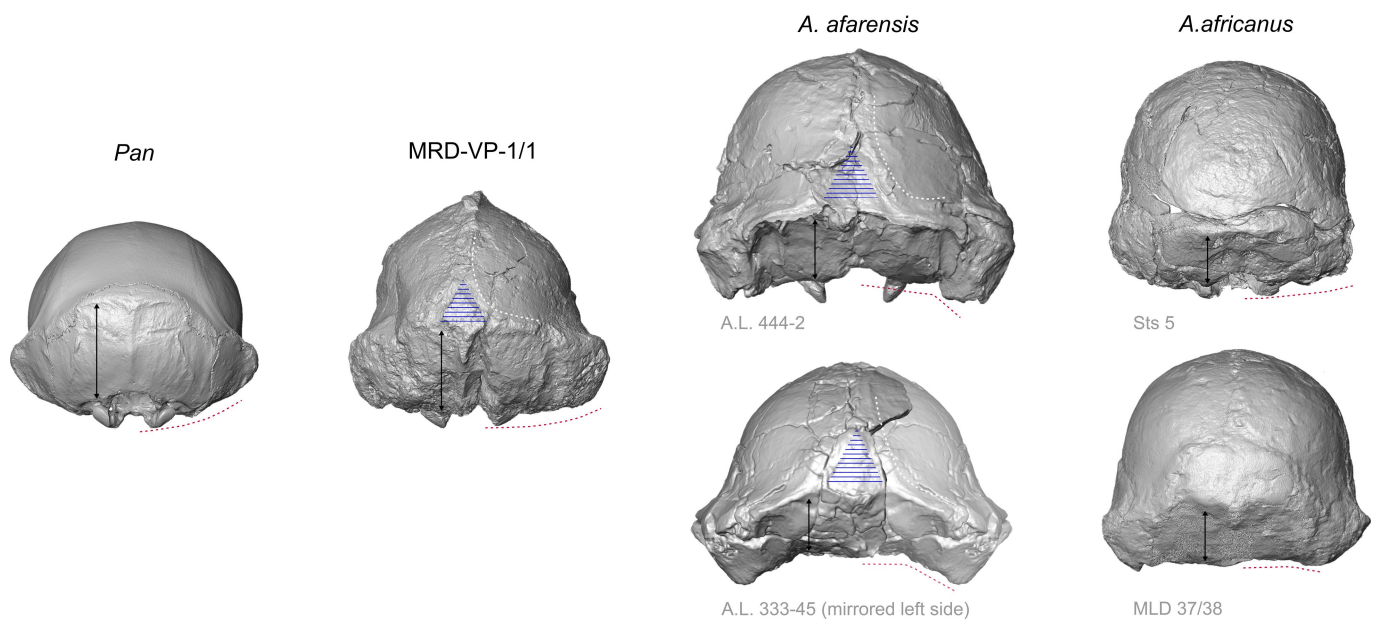
Extended Data Fig. 9 | Comparison of crania in posterior view. The transverse contour of the cranial base is convex in African apes, whereas *A. afarensis* shows an angular transition between the nuchal region and the greatly expanded mastoids (red dashed lines). In this regard, *A. afarensis* anticipates the morphology of robust australopiths, but *A. africanus* is less derived. MRD shows the primitive convex contour of the base, even though the mastoids are expanded. MRD is also primitive with regard to the great length of the nuchal plane (black arrows). However, it is similar to *A. afarensis* in the configuration of the compound temporal–nuchal crest (white dashed lines), the bare area (blue hatched triangle), and the overall 'bell-shaped' posterior outline (that is, the parietal walls are slightly convergent superiorly and the greatest width occurs basally across the enlarged mastoids).
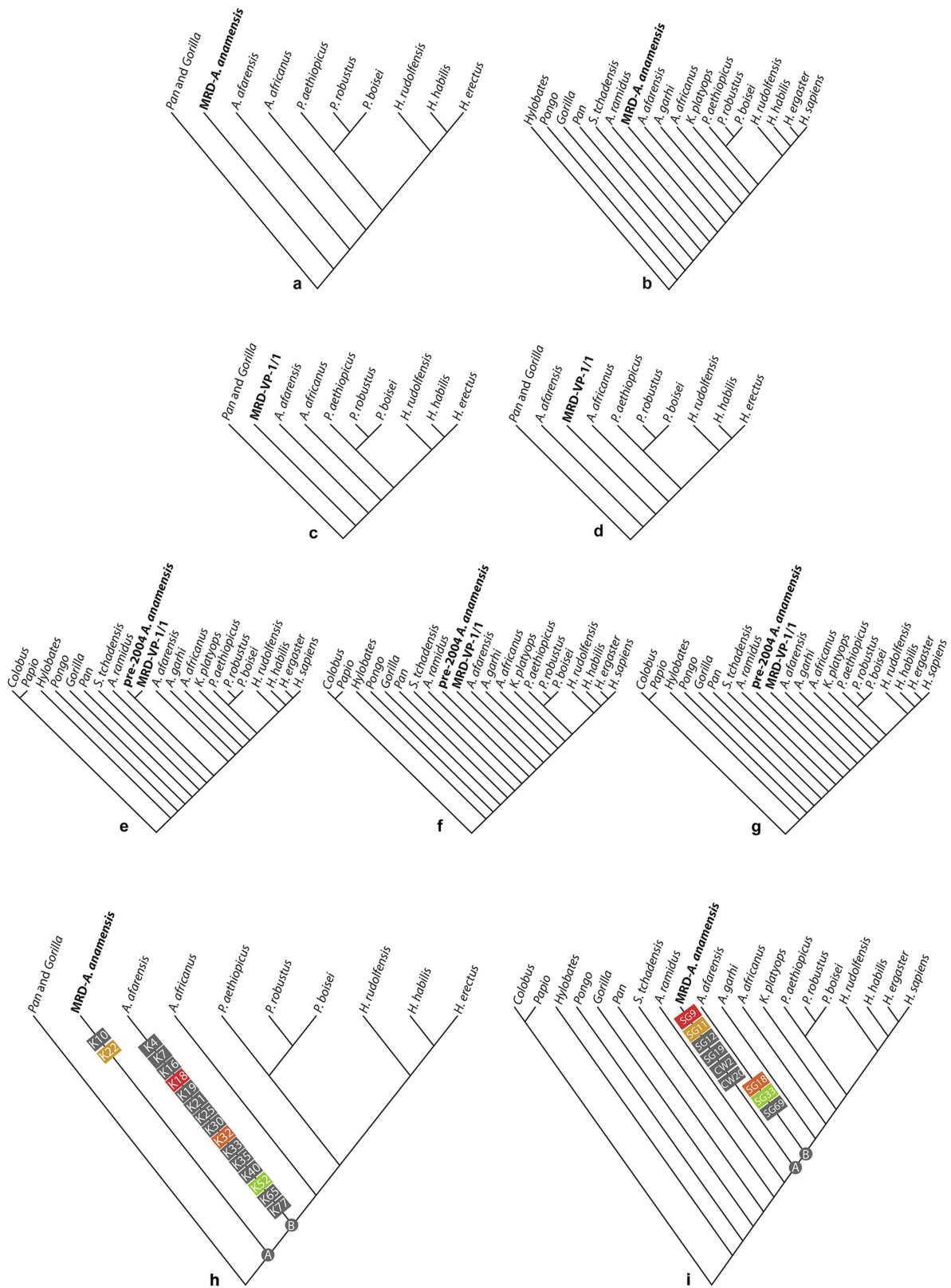
Extended Data Fig. 10 | See next page for caption.

Extended Data Fig. 10 | Results of phylogenetic analyses. a, Cladogram resulting from the character matrix of ref. [27], with the addition of MRD and previously described *A. anamensis* specimens (combined as a single OTU, K-combined). Parsimony analysis returned a single most-parsimonious tree ($l = 196$, $C = 0.71$, $R = 0.70$). **b**, Cladogram resulting from the character matrix of ref. [33] (and references therein) with the addition of the combined MRD–*A. anamensis* OTU (S&G-combined). This analysis returned a single most-parsimonious tree ($l = 429$, $C = 0.47$, $R = 0.66$) with identical topology. The position of the combined MRD–*A. anamensis* OTU reinforces accepted relationships and is consistent with geochronology. **c–g**, Cladograms resulting from analyses in which MRD is treated as a separate OTU (that is, an OTU bearing observations primarily for cranial characters, but very few dental characters and no mandibular characters.) **c**, **d**, Equally parsimonious cladograms from the K-separate analysis ($l = 196$, $C = 0.71$, $R = 0.68$). **e–g**, Equally parsimonious

cladograms from the S&G-separate analysis ($l = 430$, $C = 0.47$, $R = 0.66$). The 'pre-2004 *A. anamensis*' OTU in **e–g** bears observations primarily on dentognathic characters. Character scores for MRD are provided in Supplementary Table 1, sheets 1 and 2. Regardless of whether cranial or dentognathic characters are considered, the phylogenetic placement of MRD and the previously known *A. anamensis* sample remains stable relative to other hominins. **h**, **i**, Cladograms from the K-combined and S&G-combined analyses (as in **a** and **b**), with apomorphies added to the cladograms to illustrate the implied pattern of evolutionary change. The character states reconstructed at nodes A and B provide the reference for identifying *A. anamensis* and *A. afarensis* apomorphies, which are shown here as rectangles containing their abbreviated character labels. Characters in red, orange, gold and green describe similar morphology and appear in both previously published studies[27,33]. See Supplementary Note 9 and Supplementary Table 1.

nature research

Corresponding author(s):   Yohannes Haile-Selassie

Last updated by author(s): Jul 16, 2019

Reporting Summary

Nature Research wishes to improve the reproducibility of the work that we publish. This form provides structure for consistency and transparency in reporting. For further information on Nature Research policies, see Authors & Referees and the Editorial Policy Checklist.

Statistics

For all statistical analyses, confirm that the following items are present in the figure legend, table legend, main text, or Methods section.

n/a	Confirmed	
☐	☒	The exact sample size (*n*) for each experimental group/condition, given as a discrete number and unit of measurement
☒	☐	A statement on whether measurements were taken from distinct samples or whether the same sample was measured repeatedly
☐	☒	The statistical test(s) used AND whether they are one- or two-sided *Only common tests should be described solely by name; describe more complex techniques in the Methods section.*
☒	☐	A description of all covariates tested
☒	☐	A description of any assumptions or corrections, such as tests of normality and adjustment for multiple comparisons
☐	☒	A full description of the statistical parameters including central tendency (e.g. means) or other basic estimates (e.g. regression coefficient) AND variation (e.g. standard deviation) or associated estimates of uncertainty (e.g. confidence intervals)
☐	☒	For null hypothesis testing, the test statistic (e.g. *F*, *t*, *r*) with confidence intervals, effect sizes, degrees of freedom and *P* value noted *Give P values as exact values whenever suitable.*
☒	☐	For Bayesian analysis, information on the choice of priors and Markov chain Monte Carlo settings
☒	☐	For hierarchical and complex designs, identification of the appropriate level for tests and full reporting of outcomes
☒	☐	Estimates of effect sizes (e.g. Cohen's *d*, Pearson's *r*), indicating how they were calculated

Our web collection on statistics for biologists contains articles on many of the points above.

Software and code

Policy information about availability of computer code

Data collection	Data was collected on the original specimen or on the symmetrized reconstruction, as described in the text. Comparative data were collected from original fossils and CT scans of fossils collected from various sites in Kenya, Tanzania, and Ethiopia. Extant comparative data were collected from CT scans of Pan troglodytes (n=20) and Gorilla gorilla (n=20) crania.
Data analysis	For the micro CT-scan data analysis, we used Avizo 9.3 (ThermoFisher Scientific); Geomagic Design X (3D Systems Software srl); Viewbox 4.1 software (dHAL Software, Kifissia, Greece). For the phylogenetic analysis, we used PAUP* 3.99.164.0. Summary statistics, graphs and permutation testing were conducted in the R statistical platform version 3.5.1.

For manuscripts utilizing custom algorithms or software that are central to the research but not yet described in published literature, software must be made available to editors/reviewers. We strongly encourage code deposition in a community repository (e.g. GitHub). See the Nature Research guidelines for submitting code & software for further information.

Data

Policy information about availability of data

All manuscripts must include a data availability statement. This statement should provide the following information, where applicable:

- Accession codes, unique identifiers, or web links for publicly available datasets
- A list of figures that have associated raw data
- A description of any restrictions on data availability

We have presented most of the data in Extended Data Figures, Extended Data Tables and Supplementary Information. The data that support the findings of this study, but not included in the Supplementary Information, are available from the corresponding author upon reasonable request.

Field-specific reporting

Please select the one below that is the best fit for your research. If you are not sure, read the appropriate sections before making your selection.

☐ Life sciences ☐ Behavioural & social sciences ☒ Ecological, evolutionary & environmental sciences

For a reference copy of the document with all sections, see nature.com/documents/nr-reporting-summary-flat.pdf

Ecological, evolutionary & environmental sciences study design

All studies must disclose on these points even when the disclosure is negative.

Study description	This study describes a 3.8 Myr early hominin cranium from Ethiopia and assesses its taxonomic affinity.
Research sample	In our comparative analysis, we used originals and replicas of fossil specimens recovered from Kenya, Tanzania, Ethiopia, and South Africa.
Sampling strategy	No sample size calculation was performed. Sampling strategy was merely based on availability of fossil materials, particularly crania, from the time period of interest (3-4 million years ago).
Data collection	Data from the original specimen was collected by Y.H.S. and S.M.M. Micro-CT scan data processing and collection was conducted by T.M.R., S.B., and A.V. in collaboration with Y.H.S. and S.M.M.
Timing and spatial scale	Data collection started in the summer of 2016, followed by comparative data collection during the summer of 2017. Data on the original specimen was being collected between January and March when Y.H.S. and S.M.M. had access to the specimen before their field season. This continued until the write up of this manuscript.
Data exclusions	No data was excluded from the analysis.
Reproducibility	This is a comparative morphological description of a fossil specimen and no experiments were conducted to test repeatability.
Randomization	The comparative specimens have known taxonomic affinity and there was no randomization.
Blinding	Blinding was not relevant to this study because it was a field study not an experimental study.

Did the study involve field work? ☒ Yes ☐ No

Field work, collection and transport

Field conditions	Arid, limited tree cover, low relief river valley between high, basalt covered plateaus, and hot.
Location	Area around fossil discovery site in the Godaya River Valley of the Woranso Mille project area, Afar Region, Ethiopia (11º32'59.5" N; 40º27'54.6" E)
Access and import/export	Access and sample export followed the laws and regulations of Ethiopia and the Afar Regional state. Permission from the Authority for Research and Conservation of Cultural Heritage (ARCCH), dated November 17, 2015 (Ref. # 08/KT-69/005), allowed us to conduct field research that led to the discovery of the subject of this manuscript. The Minister of Culture and Tourism authorized the export of the original fossil (MRD-VP-1/1) to the United States for CT-scanning on May 2, 2016, Ref. # 1/A-10/354.
Disturbance	Camping, road access, heat, and sample collection provided minimal disturbance.

Reporting for specific materials, systems and methods

We require information from authors about some types of materials, experimental systems and methods used in many studies. Here, indicate whether each material, system or method listed is relevant to your study. If you are not sure if a list item applies to your research, read the appropriate section before selecting a response.

Materials & experimental systems

n/a	Involved in the study
☒	☐ Antibodies
☒	☐ Eukaryotic cell lines
☐	☒ Palaeontology
☒	☐ Animals and other organisms
☒	☐ Human research participants
☒	☐ Clinical data

Methods

n/a	Involved in the study
☒	☐ ChIP-seq
☒	☐ Flow cytometry
☒	☐ MRI-based neuroimaging

Palaeontology

Specimen provenance | The specimen was collected from Woranso-Mille Site, Lead Author's field site in the Afar region of Ethiopia. Field work at the site is conducted with permits from the Authority for Research and Conservation of Cultural Heritage of the Ministry of Culture and Tourism of Ethiopia issued on November 17, 2015, Ref. # 08/KT-69/005.

Specimen deposition | The original specimen is housed in the Paleoanthropology Laboratory of the National Museum of Ethiopia.

Dating methods | Age of the specimen was determined by using 40Ar/39Ar dating of volcanic tuffs at the Berkeley Geochronology Center, located in Berkeley, California. The methods are described in a companion manuscript.

☒ Tick this box to confirm that the raw and calibrated dates are available in the paper or in Supplementary Information.